Intensity dependence in the dissociation branching ratio of ND^+ using intense femtosecond laser pulses

J. McKenna, A. M. Sayler, B. Gaire, Nora G. Johnson, E. Parke, K. D. Carnes, B. D. Esry, and I. Ben-Itzhak
J.R. Macdonald Laboratory, Kansas State University, Manhattan, Kansas 66506, USA
(Received 21 December 2007; published 25 June 2008)

We investigate the dependence of the dissociation branching ratio of ND^+ on intensity in the strong-field regime. ND^+, unexplored previously using an intense laser, offers an interesting, alternating sequence of dissociation limits to $N^+ + D$ and $N + D^+$ separated by less than the photon energy at 795 nm wavelength. By exposing an ND^+ beam to a 40 fs Ti:sapphire laser pulse and measuring the ion fragments in coincidence with the neutral fragments, we find that the branching ratio of the final dissociation channel depends strongly on intensity in the range $2\times10^{13}-3\times10^{15}$ W/cm^2. Furthermore, we use measurements of the kinetic energy release and angular distributions for these channels to identify their most probable dissociation pathways.

DOI: 10.1103/PhysRevA.77.063422 PACS number(s): 33.80.Wz, 42.50.Hz

I. INTRODUCTION

Since the ground-breaking work of Zewail [1], it has been an ambition of physicists, chemists, and biologists to use femtosecond infrared and optical laser pulses to control the outcome of a chemical reaction. This emergent field of "femtochemistry" has developed considerably in the past two decades following vast improvements in laser technology and techniques. These improvements have led to shorter, more intense pulses, with the added ability to pulse shape [2] and stabilize and control the pulse's carrier-envelope phase (CEP) [3]. Recently CEP has been used to guide the direction of electron emission from atoms [4,5] and applied to molecules, demonstrating control over a strong left-right asymmetry in the breakup of D_2^+ [6]. Moreover, CEP effects have also been predicted for simple heteronuclear systems [7,8].

Despite the enormous steps taken toward the goal of understanding and controlling molecular dynamics, one continuing difficulty in the study of the dissociation of even simple molecules is the measurement process itself. For example, to extract clear information on the dissociation of a typical molecular ion, AB^+, that dissociates via the channels,

$$AB^+ + n\omega \rightarrow A + B^+, \tag{1}$$

$$AB^+ + n\omega \rightarrow A^+ + B, \tag{2}$$

where $n\omega$ represents the interaction with the laser field, one needs to be able to discern between paths (1) and (2). Conventionally, measurement of the charged fragment product has proven straightforward as this can readily be extracted and detected, even for gas target studies, using an electrostatic field. Indeed insightful new techniques including cold-target recoil-ion momentum spectroscopy (COLTRIMS) [9] have refined measurement of the ion to very high momentum resolution. However, detection of the charged fragment by itself proves inadequate to clearly separate the channels as an alternative path for the formation of the ion is via the ionization channel:

$$AB^+ + n\omega \rightarrow A^+ + B^+ + e^-. \tag{3}$$

Thus distinguishing paths (1) and (2) from path (3) can prove challenging. Even a coincident measurement of both charged fragments to clearly identify ionization events, accompanied by subtraction of the ionization signal from the total yield, will often leave a high level of uncertainty in the dissociation yield—particularly if the probability of ionization is comparable or dominant, with respect to dissociation.

In a recent publication [10] we describe a coincidence 3D imaging technique whereby kinematically complete measurements of the dissociation of molecular ion beams are performed. The key strength of this method is that the initial velocity of the target enables the detection of both the neutral and charged dissociation fragments in coincidence thus eliminating the problem described above. This method has the additional advantage of enabling one to perform complementary work to neutral target studies by opening up a new range of ionic targets to investigate. In this paper we apply this method to generate the first measurements of intense-field dissociation of ND^+.

The NH^+ radical is an important astrophysical species as it is believed to play a vital role in the synthesis of ammonia in dense interstellar media [11], as well as being formed by various reaction mechanisms in other environments such as the gas tail of comets [12] (see Ref. [13] for a brief review). So far, however, the search for it in space has been unfruitful. Nevertheless, a number of spectroscopy-style measurements [14–17], as well as theoretical works on the electronic structure of NH^+ [13,18–23], have been performed over the years leading to relatively detailed information on its molecular structure.

From an intense-field perspective, ND^+ is an interesting target to probe as it has an alternating sequence of dissociation limits into (a) $N^+ + D$ and (b) $N + D^+$ (see Fig. 1), each spaced in energy by between 0.3 and 1.5 eV, just less than one photon energy at 795 nm wavelength (1.56 eV). Thus we pose the question: how does the branching ratio of these dissociation channels depend on the laser field strength? This query is timely since much emphasis is currently placed on selectively determining the outcome of a particular reaction mechanism. Indeed, ND^+ would seem a target well suited for future studies on state-selective control of dissociation. In this paper we address the question of the $N^+ + D$ and $N + D^+$ dissociation branching ratio intensity dependence and discuss the intense-field dissociation dynamics of this molecule.

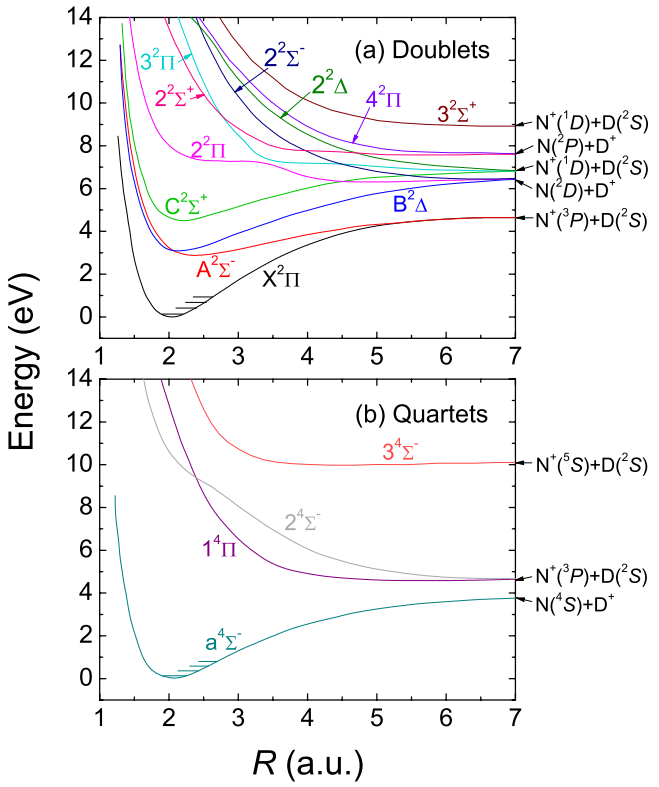

FIG. 1. (Color online) Potential energy curves of ND^+ for the lowest-lying (a) doublet and (b) quartet states. Potential energy is given with respect to the bottom of the ground $X^2\Pi$ state well. Computed energies for the lowest few vibrational states are indicated by horizontal lines. Curves have been reproduced from Ref. [18].

II. METHOD

Details on the experimental technique used have been offered elsewhere [10,24], hence only the salient points will be relayed here. The ND^+ ions are formed from deuterated ammonia (ND_3) by electron impact ionization in an electron cyclotron resonance (ECR) ion source. They are formed as a mixture of ground $X^2\Pi$ and metastably excited $a^4\Sigma^-$ states, although the ratio of these populations is unknown. The ND^+ ions are extracted and momentum selected using electrostatic and electromagnetic fields, respectively, forming a well-collimated 9 keV ND^+ beam. In the interaction region the ion beam is crossed at 90° with a focused laser beam. The polarization direction is chosen to be oriented orthogonal to the ion-beam propagation direction. The dissociation fragments, resulting from the laser interaction, continue along in the general direction of the primary ion beam to a position sensitive delay-line detector (80 mm diameter). The primary ND^+ beam is collected in a small on-axis Faraday cup (2 mm diameter) near the center of the detector. Due to the large mass difference of N and D (ratio 7:1), slow nitrogen fragments may be blocked by the Faraday cup while fast deuterium fragments may travel outside the detector face. We estimate that our setup allows the kinetic energy release (KER) to be measured in the range $0.1 < \mathrm{KER} < 3.3$ eV. The position and time-of-flight information of the particle hits on the detector are used to determine the three-dimensional momentum of each dissociative fragment. In the interaction region there is an additional weak electrostatic field applied in the direction of the ion beam. This field acts to accelerate the charged fragments and thus separate them in flight time from the neutrals. A coincidence measurement is therefore achieved as illustrated in Fig. 2. This correlation spectrum, showing a plot of the flight time of the first particle to arrive at the detector vs that of the second for those event pairs that conserve momentum, illustrates precisely the importance and power of the coincidence measurement. Momentum conservation enforced by the two-body breakup of ND^+ cleanly distinguishes real events from background particle hits on the detector. In Fig. 2 each of the channels, conforming to path Eqs. (1)–(3) (where $A \equiv \mathrm{N}$ and $B \equiv \mathrm{D}$), are clearly identifiable and separable. Therefore we may precisely determine the branching ratio of the dissociation channels for a given intensity measurement.

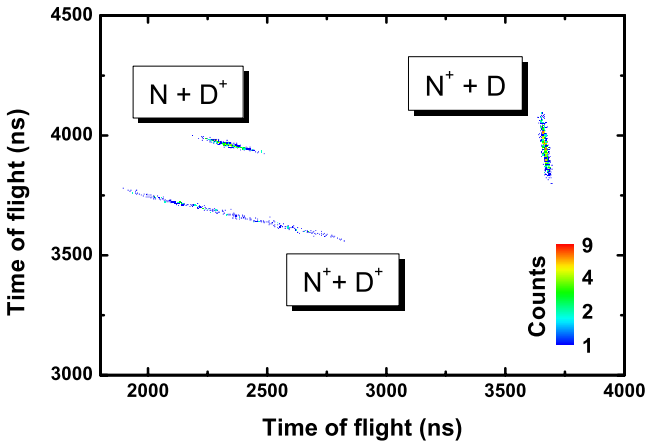

FIG. 2. (Color online) Coincidence time-of-flight spectrum for the dissociation and single ionization fragmentation channels of ND^+ plotted as the flight time of the first particle to arrive at the detector vs the flight time of the second, for particle pairs that conserve momentum.

The laser used in this study was a Kerr-lens mode-locked Ti:sapphire system (795 nm central wavelength) providing 40 fs, 1.6 mJ pulses at 1 kHz repetition rate. These pulses were focused on target using an off-axis parabolic mirror ($f = 203$ mm) mounted on a micrometer translation stage. The focus of the laser, with a peak intensity of $I_0 \sim 2.6 \times 10^{15}$ W/cm^2, was scanned parallel to the laser propagation direction (along the z axis) employing an intensity selective scan method [25,26]. At each z position the thin ion-beam target (cross section $\sim 0.5 \times 0.6$ mm^2) intersected the laser path at a different portion of its focal volume. Thus as one scanned the interaction volume away from the center of the laser focus, the ion-beam progressively experienced a decreasing intensity. The input pulse energy was maintained constant throughout. In this way the intensity of interaction could be controlled in a precise manner with the advantage that the signal from the low intensity interaction steps was enhanced by the increased interaction volume with the less tightly focused laser. This volume enhancement does not affect the branching ratio of the different dissociation channels as the volume is the same for each channel within a single measurement.

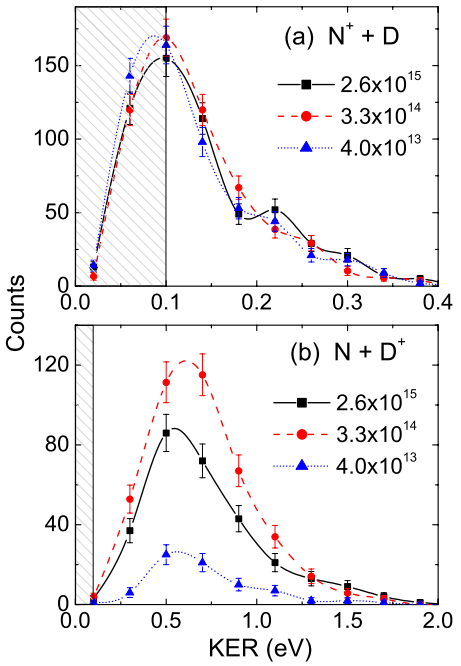

FIG. 3. (Color online) (a) Kinetic energy release (KER) distribution spectra for the dissociation of ND^+ in (a) $N^+ + D$ (KER $\sim 0.0-0.4$ eV) and (b) $N + D^+$ (KER $\sim 0.0-2.0$ eV) at intensities indicated (in units of W/cm^2). The total number of counts in the spectra of (a) have been normalized to one another. The same normalization factors are used in spectra (b). The shaded regions denote regions of expected loss due to the Faraday cup; see text for details.

III. RESULTS AND DISCUSSION

Shown in Figs. 3(a) and 3(b) are the KER distribution spectra for the dissociation of ND^+ into channels (a) $N^+ + D$ and (b) $N + D^+$, respectively, at a selection of intensities. The total number of dissociation events for channel $N^+ + D$ [Fig. 3(a)] have been normalized to one another for each of the intensities. The counts of the competing $N + D^+$ channel [Fig. 3(b)] are shown relative to the respective $N^+ + D$ count. By taking the ratio of the total counts in the spectra for each channel, to the total number of dissociation events, we obtain the branching ratio of these channels. The shaded areas of the spectra denote possible regions of loss in the distributions where low momenta N and N^+ fragments may be blocked by the Faraday cup (see discussion in Sec. II). In the case of $N^+ + D$, where the KER is observed to be small, events below 0.1 eV can be lost due to the blocked N^+ fragments. Thus the question of where the KER distribution actually peaks (between 0.0 and 0.1 eV) remains open for future studies.

Before embarking on how to decipher the dissociation pathways from the spectra, we remark on a few intriguing aspects of the data. First, one may have noted the large difference in KER range for the two channels; $N^+ + D$ spans approximately the 0.0–0.4 eV range, while $N + D^+$ spans approximately the 0.0–2.0 eV range. The difference in the KER range can be attributed to the dissociation pathway leading to that specific channel which we identify in the upcoming discussion. Also intriguing is the narrow energy spread of the peaks, particularly for $N^+ + D$ (~ 0.1 eV FWHM). As we will show, we believe the population of the ground state of ND^+ is almost entirely in a single vibrational level ($v=0$) for these experiments. Therefore there is little spread in the final energy distribution as the initial state of the system is well defined. Second, the absence of any higher KER dissociation peaks (>1.0 eV), which may be considered atypical for other small diatomic molecules (e.g., O_2^+ [27]), is due to the shallow nature of the electronic states involved in the dissociation. Referring back to Fig. 1(a), we observe that for the doublet states all of the lowest-lying potential curves are either attractive, or only shallow repulsive, for internuclear distance $R>2$ a.u. Therefore dissociation on these potentials is likely to lead to low energy release. Finally, it was observed in these experiments that the total rate of ND^+ dissociation at the highest intensity (2.6×10^{15} W/cm^2) was more than one order of magnitude lower than for H_2^+ dissociation under similar laser and ion-beam conditions, indicating that ND^+ is difficult to dissociate because of the large number of photons involved.

To determine the likely dissociation paths of ND^+ leading to the products $N^+ + D$ and $N + D^+$, we will draw on knowledge gained from our previous work on small diatomic molecules [27]. In that paper we outlined a set of guidelines that may be used to identify the likely dissociation path. Here we apply those rules to ND^+. For example, we know, assuming the spin-orbit coupling is negligible, that the doublet and quartet states of ND^+ (Fig. 1) will not be mixed by the laser interaction due to spin-transition selection rules, i.e., a transition from a doublet to a quartet state, or vice versa, would require a spin flip of an electron which is very improbable. Thus these systems may be treated independently, simplifying greatly the total number of possible dissociation routes. Also, the transition probability strongly favors those transitions requiring fewer total number of absorbed photons, hence we can confidently rule out high-lying excited states from playing a major role in the dissociation process.

To the best of our knowledge, the exact vibrational population distribution of the $X^2\Pi$ and $a^4\Sigma^-$ states of ND^+ prepared from ammonia through electron-impact (i.e., $ND_3 + e^- \rightarrow ND^+ + D_2 + 2e^-$) is unknown. However, since the equilibrium N–D bond length of ND_3 is 1.91 a.u. [28], which is close to that of the ND^+ $X^2\Pi$ (2.02 a.u.) and $a^4\Sigma^-$ (2.06 a.u.) states [18], the population is likely to be relatively low-lying. Using a model potential energy surface cut for the N–D bond of ammonia [28], and applying a Franck-Condon projection of its ground state wave function onto the ND^+ states, we estimate the vibrational population to be mostly ($\sim 90\%$) in the $v=0$ state of the $X^2\Pi$ and/or $a^4\Sigma^-$ electronic states. This is consistent with the narrowness of the observed KER distributions, particularly that in Fig. 3(a). Hence ND^+ prepared in this way seems to be a nice example of a vibrationally cold target. Indeed, achieving ground vibrational state molecular ions has been a goal for some time for intense-field studies and has only recently been demonstrated for HD^+ by using an electrostatic storage device [29]. The effect of having a very low-lying vibrational population is that for ND^+ to dissociate directly via the high-lying doublet ($3^2\Pi$, $2^2\Sigma^-$, $2^2\Delta$, $2^2\Sigma^+$, $4^2\Pi$, $3^2\Sigma^+$) and quartet ($1^4\Pi$, $2^4\Sigma^-$, $3^4\Sigma^-$) states would require the absorption of many photons (approxi-

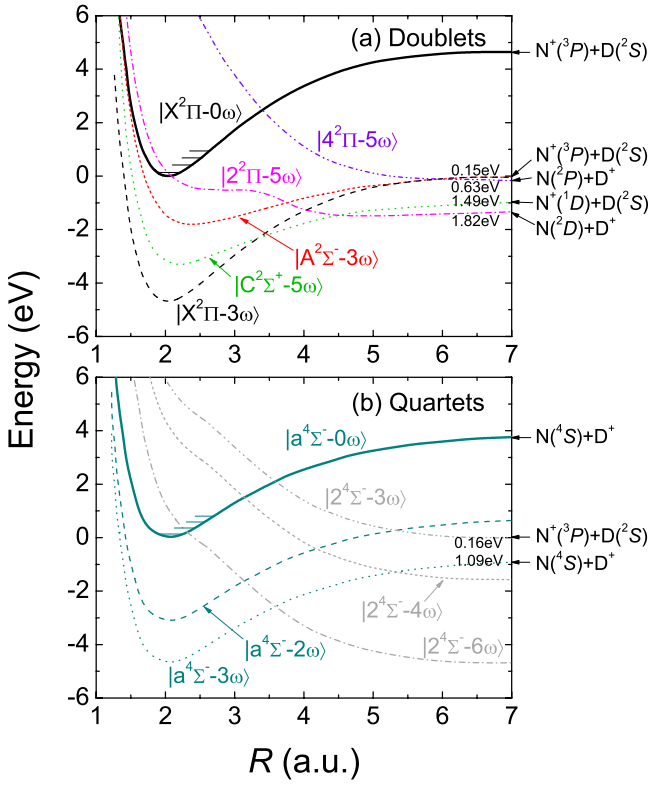

FIG. 4. (Color online) A selection of dressed potential energy curves of ND^+ for the (a) doublet and (b) quartet states. Computed energies for the lowest few vibrational states are indicated by horizontal lines. The numbers adjacent to certain dissociation limits correspond to the expected kinetic energy release for dissociation from that state starting from the $v=0$ vibrational level of the $X^2\Pi$ or $a^4\Sigma^-$ states. Field free curves have been reproduced from Ref. [18].

mately 7–11), which renders vertical transitions to these states unlikely. In addition, the centroid of the observed KER distributions (Fig. 3) is inconsistent with the highly repulsive nature of these states which should lead to a KER $\gg 1$ eV. This is not observed in Fig. 3.

To further narrow down the dissociation paths, we consider individually all remaining dissociation paths and eliminate one by one those that are inconsistent with the data. To do so we employ the dressed states Floquet approach (e.g., Refs. [27,30]) as an easier visualization of the dissociation routes. This approach, however, is equivalent to the alternative representation often used (e.g., Ref. [31]), where excitations between states are indicated as vertical transitions, resonant with an integer number of photons. In the dressed states method the potential energy curves for all electronic states (Fig. 1) are "dressed" downwards (or upwards) in energy by the number of absorbed (or emitted) photons, $n\omega$—e.g., $|X^2\Pi-3\omega\rangle$ refers to the $X^2\Pi$ state shifted down in energy by the absorption of three photons. Thus each state repeats itself periodically in energy, separated by multiples of the photon energy (1.56 eV). Here we have assumed the transition dipole to be significant allowing all photon numbers to be associated with each state which for a light system like ND^+ is a reasonable assumption. In Fig. 4, to save congestion, we plot only the dressed potential energy curves that we have identified as relevant dissociation pathways for the doublet and quartets states of ND^+. Where the curves cross one another the laser-induced coupling of the states is largest, and the crossings are avoided, giving the largest transition probability. The transition probability decreases rapidly as the distance from the crossing increases.

A. N^++D pathway

For N^++D, we observe that the KER distribution is peaked at, or below, 0.1 eV [see Fig. 3(a)], with an uncertainty in the exact value due to losses by the Faraday cup. Energetically, the dissociation KER of a channel is given by the difference in energy of the initial and dressed final states of the molecule. Hence for N^++D the dressed dissociation limit must be near equipotential with the bottom of the undressed $X^2\Pi$ or $a^4\Sigma^-$ wells (since the vibrational population of both is deeply bound, mostly in the $v=0$ vibrational state shown). For the doublets [Fig. 4(a)], the only possible final states that conform to this restriction are the $|A^2\Sigma^- - 3\omega\rangle$ and $|X^2\Pi - 3\omega\rangle$ states—both resulting in a KER of about 0.15 eV (as they share the same dissociation limit), in relatively close agreement with the data. This expected value is calculated from the energy difference between $v=0$ and the dressed dissociation limit at $R=\infty$. Indeed, one may expect a small shift of the KER to lower energy as the $v=0$ state may get Stark-shifted downwards in energy by the laser field, giving better agreement with the observed value. The $|C^2\Sigma^+ - 5\omega\rangle$ or $|3^2\Pi - 5\omega\rangle$ states can be ruled out as they would result in too large of a KER value ($\sim$1.49 eV). However, neither the dressed $A^2\Sigma^-$ nor the $X^2\Pi$ state forms a direct curve crossing with the bottom of the undressed ground state well. Thus for a dissociative wave packet starting near $v=0$ to reach either of these final states it must first make a transition through an intermediate state. The most suitable candidate is the $|2^2\Pi - 5\omega\rangle$ state, which forms an avoided crossing with the $|A^2\Sigma^- - 3\omega\rangle$ state at $R=3.7$ a.u., and the $|X^2\Pi - 3\omega\rangle$ state at $R=4.0$ a.u. Hence the bound ND^+ molecule first absorbs five photons to get excited to the $2^2\Pi$ state, before re-emitting two photons to transit onto the $A^2\Sigma^-$ or $X^2\Pi$ states.

To distinguish between the $A^2\Sigma^-$ and $X^2\Pi$ states, one may look at the angular distribution of the fragments. The expected angular distribution may be described using a simple model [27,32] as $\cos^{2n}\theta \sin^{2m}\theta$, where θ is the angle between the $[N-D]^+$ molecular axis and the laser polarization, and n and m refer to the number of absorbed or emitted photons during parallel (e.g., $\Pi\rightarrow\Pi$, $\Sigma\rightarrow\Sigma$) or perpendicular (e.g., $\Pi\rightarrow\Sigma$, $\Sigma\rightarrow\Pi$) transitions, respectively. Hence the $X^2\Pi \rightarrow |2^2\Pi - 5\omega\rangle \rightarrow |A^2\Sigma^- - 3\omega\rangle$ transition should give, roughly, a $\cos^{10}\theta \sin^4\theta$ distribution, whereas the $X^2\Pi \rightarrow |2^2\Pi - 5\omega\rangle \rightarrow |X^2\Pi - 3\omega\rangle$ transition gives, roughly, a $\cos^{14}\theta$ distribution. In Fig. 5(a) the measured angular distribution of N^++D is displayed. We note that there is a higher level of uncertainty in the data at 90° emission angle as those particles are most susceptible to losses from the Faraday cup. Nevertheless, clearly the distribution is not peaked along the laser polarization, indicating that the pathway involving the $A^2\Sigma^-$ state is likely to be dominant.

Even though inclusion of perpendicular transitions improves the agreement between our model and the experi-

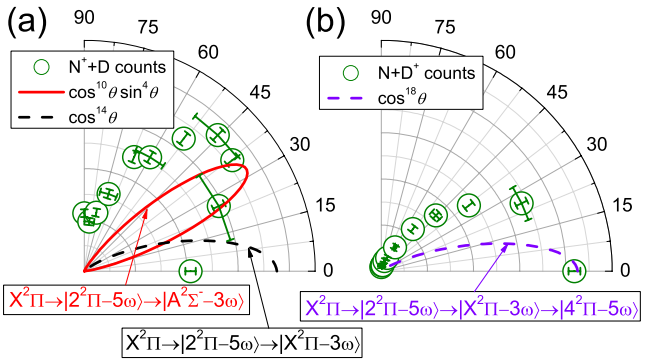

FIG. 5. (Color online) The measured angular distributions of ND^+ for (a) $N^+ + D$ and (b) $N + D^+$. The data points with error bars denote observed distributions, and the lines denote model distributions for the transitions indicated.

ment, there is still a clear discrepancy both in the angle at which the distributions are peaked, and in the width of the distributions. There are a number of possible reasons that may contribute to this difference. First of all, the low KER of this channel means that the N^+ fragments form a small spatial distribution near the center of the position-sensitive detector. This leads to a relatively large level of uncertainty in the angular measurement. We estimate this uncertainty using a method implemented elsewhere [33], denoting the uncertainty by error bars (in angle) added to select data points in Fig. 5. These alone do not fully account for the difference. Another source for the difference could be the simplicity of the model used to generate the fit which neglects interference terms from different transitions. Namely, in the model, we use an incoherent sum over the pathways rather than the more correct coherent sum. Explicitly, the angular probability distribution is approximated by taking the sum of the squared transition amplitude for each pathway, as opposed to the square of the sum over all transitions. Thus the cross terms that give rise to interference are omitted. Such interference may act to slightly broaden or skew the actual distribution. Last, the difference may be an indication of weaker contributions from alternative pathways that also involve a mixture of parallel and perpendicular transitions.

An alternative path that would also produce low KER $N^+ + D$ fragments involves the quartet states. As shown in Fig. 4(b), the transition sequence $a^4\Sigma^- \rightarrow |2^4\Sigma^- - 6\omega\rangle \rightarrow |a^4\Sigma^- - 2\omega\rangle \rightarrow |2^4\Sigma^- - 3\omega\rangle$ will give a KER of about 0.16 eV. However, each step of the sequence involves a $\Sigma \rightarrow \Sigma$ transition hence the total angular distribution, like the $|X^2\Pi - 3\omega\rangle$ distribution, would be expected to be strongly peaked along the laser polarization which is inconsistent with the data shown in Fig. 5(a).

A further mechanism that must be considered is direct excitation of $X^2\Pi$ ($v=0$) to the continuum due to the permanent dipole moment of ND^+. This could proceed through the absorption of three photons ($|X^2\Pi - 3\omega\rangle$) and would result in KER=0.15 eV. However, as this mechanism involves a direct $\Pi \rightarrow \Pi$ coupling the dissociation fragments should be aligned with the laser polarization ($\cos^6\theta$), hence once more we can exclude this mechanism on the basis of its angular distribution. Furthermore, we believe the probability of this mechanism occurring at this wavelength to be small. We therefore, through process of elimination, conclude that the $X^2\Pi \rightarrow |2^2\Pi - 5\omega\rangle \rightarrow |A^2\Sigma^- - 3\omega\rangle$ pathway must be the dominant dissociation mechanism leading to $N^+ + D$.

B. $N + D^+$ pathway

A similar logic may be applied to unravel the dominant mechanism in the case of $N + D^+$. This channel has a KER distribution peaked at about 0.6 eV, with a FWHM value of ~0.6 eV. For dissociation to the $N + D^+$ limit, the $B^2\Delta$ state is not appropriate as it resembles closely the shape and equilibrium bond length of the ground $X^2\Pi$ state, and thus, even when dressed by the laser field, it remains difficult to dissociate from. Likewise, the $A^2\Sigma^-$ and $C^2\Sigma^+$ states have bound-shaped potentials, albeit shallower than the $B^2\Delta$ state, and so do not make for good intermediate states in aiding dissociation. As was observed for $N^+ + D$, the $2^2\Pi$ state leading to $N(^2D) + D^+$ can be accessed directly from the ground state by the laser and so, at first sight, may seem the most appropriate dissociation path. However, as Fig. 4(a) indicates the resultant KER would be approximately 1.82 eV which is much larger than the observed value. If one lowers the next available $N(^2P) + D^+$ dissociation limit, by the absorption of five photons, the expected KER of about 0.63 eV is in excellent agreement with the observed value. Two possible final states lead to this limit, that is, the $2^2\Sigma^+$ and $4^2\Pi$ levels. To reach either of this states from $v=0$, dissociation would have to first proceed via $|2^2\Pi - 5\omega\rangle$, followed by a transition to either $|A^2\Sigma^- - 3\omega\rangle$ or $|X^2\Pi - 3\omega\rangle$, with a final transition to the $|2^2\Sigma^+ - 5\omega\rangle$ and $|4^2\Pi - 5\omega\rangle$ states. As the observed angular distribution in Fig. 5(b) is peaked in the direction of the laser polarization, this suggests each step of the dissociation pathway must involve parallel transitions, pointing toward the $4^2\Pi$ state as the dominant one, i.e., $X^2\Pi \rightarrow |2^2\Pi - 5\omega\rangle \rightarrow |X^2\Pi - 3\omega\rangle \rightarrow |4^2\Pi - 5\omega\rangle$ giving, roughly, a $\cos^{18}\theta$ distribution. While the observed and predicted angular distributions [Fig. 5(b)] agree well in terms of the main dissociation direction, the observed distribution is much broader than the model prediction, as was also the case for $N^+ + D$.

An alternative possible dissociation path for $N + D^+$ would be dissociation to the $|a^4\Sigma^- - 3\omega\rangle$ state, leading to products $N(^4S) + D^+$. The KER value, however, in this case would be about 1.09 eV, i.e., approximately 0.5 eV larger than where the observed distribution is peaked. This indicates that this state is not the dominant path although one may not rule out the possibility that it contributes to the high KER tail of the distribution at KER > 1.0 eV.

C. Branching ratios

Having established the most probable dissociation paths, we now pursue the main goal of this work, that is, to examine the dependence of the $N^+ + D$ and $N + D^+$ branching ratios on laser intensity. Before doing so, we display the dissociation rates for the $N + D^+$ and $N^+ + D$ channels as a function of intensity in Fig. 6(a), both normalized to the ion-beam current. With decreasing intensity the interaction volume with the laser increases, due to the intensity selective scan method we use, while the dissociation probability is likely to de-

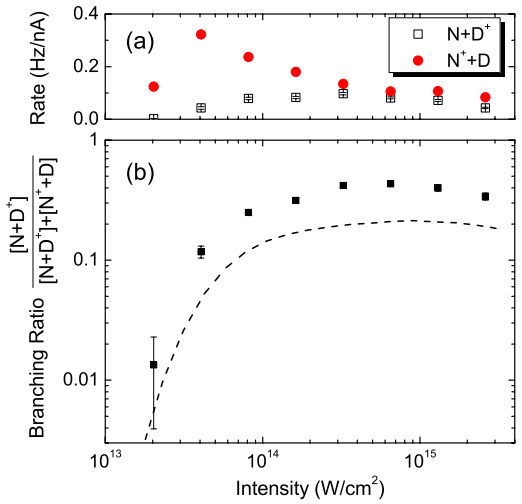

FIG. 6. (Color online) (a) Rates for the dissociation channels $N+ D^+$ (open squares) and $N^+ + D$ (solid circles) as a function of intensity, normalized to the ion-beam current. Statistical error bars are within the size of the symbols. (b) Branching ratio for dissociation of the $N+ D^+$ channel. The dashed curve is a lower limit estimate of the absolute value of this ratio allowing for Faraday cup losses and detection efficiency (see text).

crease. The observed variation of the dissociation rates is therefore a convolution of these two factors. From these rates we obtain the branching ratios for these dissociation channels. The results for the branching ratio of the $N+D^+$ channel are displayed in Fig. 6(b) as the ratio of the number of $N+D^+$ counts to the total number of dissociation counts. This ratio has been measured over the intensity range $2\times10^{13}-3\times10^{15}$ W/cm^2. While there is some uncertainty in the absolute magnitude of this branching ratio due to a possible loss in counts of $N^+ + D$ below KER=0.1 eV, this should not affect the relative change in the ratio from one intensity to another. This follows from the fact that the overall shape of the $N^+ + D$ KER distribution [Fig. 3(a)] is insensitive to laser intensity, thus any percentage loss at one intensity will be the same for all intensities. Should there be a loss, this will act to decrease the overall magnitude of the ratio. The ratio may decrease further by the lower detection efficiency of the D fragment compared to D^+, but again will not affect the trend of the ratio as a function of intensity. By estimating the maximum loss of counts for $N^+ + D$ [34], and accounting for the difference in detection efficiencies, we plot on the figure a lower limit for the ratio, shown by the dashed curve.

The clear trend of the branching ratio is a rapid decrease in the relative number of $N+D^+$ counts for intensities below 10^{14} W/cm^2. This trend is also observed directly in the raw data, as $N+D^+$ is seen to effectively "switch off" at lower intensities. Qualitatively, the result indicates that it is more difficult to dissociate to $N+D^+$ than $N^+ + D$, thus requiring higher intensity. This conclusion is consistent with our assignment of dissociation pathways since we found that the $4^2\Pi$ state leading to $N+D^+$ requires absorption of 2 photons more than the $A^2\Sigma^-$ state that gives $N^+ + D$. The branching ratio tends to flatten off beyond an intensity of $\sim3\times10^{14}$ W/cm^2 suggesting that both channels reach saturation. We note that at the highest intensities the branching ratio decreases slightly, observed also in Fig. 3(b). At these intensities the dissociation dynamics will be complicated by the opening of new dissociation paths, and the onset of ionization which we see above $\sim5\times10^{14}$ W/cm^2.

Recently, Korolkov *et al.* [35] reported a similar study into the intensity-dependent branching ratio of DCl^+. Deuterium chloride, like ND^+, is an interesting system where the lowest dissociation limits into $D^+ + Cl$ and $D + Cl^+$ are separated by ~0.9 eV (less than one 800 nm photon), the latter being the lower limit. Korolkov *et al.* find a similar intensity dependence for the branching ratio of D^+/Cl^+ to that reported here for ND^+. However, their study was hampered by the fact that they started from a neutral gas target of DCl (rather than an ion-beam of DCl^+) which subsequently limited the range of intensities they could study due to the need to first form the DCl^+ molecules, and then dissociate them, within the same laser pulse. Moreover, there were additional effects that inhibited a direct measurement of the DCl^+ dissociation branching ratio. For example, Korolkov *et al.* found that the intensity that gave maximum rate of change in the branching ratio depended sensitively on the chirp of the laser pulse. They attributed this to the fact that different chirps would populate the DCl^+ molecule in a different range of initial vibrational states, which affects the branching ratio. In our study this effect is circumvented as the ND^+ ions are formed by electron-impact in the ion source, and furthermore, they form a vibrationally cold target. In addition, in the DCl^+ experiment, the branching ratio was inferred from the ratio of the D^+/Cl^+ ions formed. However, ionization to DCl^{2+} followed by decay into $D^+ + Cl^+$ would inherently have an adverse effect on the branching ratio. Such an example underlines the advantage of the method used here where the dissociative fragments (both ion and neutral) are measured in coincidence.

IV. SUMMARY

In summary, we have presented a concise analysis of the intense-field dissociation of the astrophysically important species, ND^+. To enable a clean measurement of the branching ratio of the two possible dissociation channels, $N^+ + D$ and $N+D^+$, we employed a kinematically complete, coincidence 3D imaging technique. It also allowed us to map the kinetic energy release and angular distributions of each channel. These distributions lead us to conclude that, in the intensity range $2\times10^{13}-3\times10^{15}$ W/cm^2, dissociation is most likely dominated by the $X^2\Pi$ ground state of ND^+, proceeding via the $A^2\Sigma^-$ state for production of $N^+(^3P)+D(^2S)$, and the $4^2\Pi$ state for production of $N(^2P)+D^+$. The ratio of the two dissociation channels was found to be very sensitive to intensity, the $N+D^+$ channel dropping rapidly in rate with decreasing intensity below $\sim10^{14}$ W/cm^2. This work has presented a clear method of identifying the different dissociation pathways of a molecular ion which should aid selective control of the dissociation channel (e.g., by using the carrier-envelope phase of the laser pulse), as control becomes more feasible in the near future.

ACKNOWLEDGMENTS

The authors wish to thank Professor Z. Chang and his group members for providing the laser beam and Dr. C. Fehrenbach for assistance with the ion beam. This work was supported by the Chemical Sciences, Geosciences, and Biosciences Division, Office of Basic Energy Sciences, Office of Science, U.S. Department of Energy.

[1] A. H. Zewail, Science **242**, 1645 (1988).
[2] A. M. Weiner, Rev. Sci. Instrum. **71**, 1929 (2000).
[3] A. Baltuska *et al.*, Nature (London) **421**, 611 (2003).
[4] G. G. Paulus, F. Lindner, H. Walther, A. Baltuska, E. Goulielmakis, M. Lezius, and F. Krausz, Phys. Rev. Lett. **91**, 253004 (2003).
[5] F. Lindner, M. G. Schätzel, H. Walther, A. Baltuska, E. Goulielmakis, F. Krausz, D. B. Milosevic, D. Bauer, W. Becker, and G. G. Paulus, Phys. Rev. Lett. **95**, 040401 (2005).
[6] M. F. Kling *et al.*, Science **312**, 246 (2006).
[7] V. Roudnev, B. D. Esry, and I. Ben-Itzhak, Phys. Rev. Lett. **93**, 163601 (2004).
[8] G. L. Kamta and A. D. Bandrauk, Phys. Rev. Lett. **94**, 203003 (2005).
[9] J. Ullrich, R. Moshammer, A. Dorn, R. Dörner, L. Ph. H. Schmidt, and H. Schmidt-Böcking, Rep. Prog. Phys. **66**, 1463 (2003).
[10] I. Ben-Itzhak, P. Q. Wang, J. F. Xia, A. M. Sayler, M. A. Smith, K. D. Carnes, and B. D. Esry, Phys. Rev. Lett. **95**, 073002 (2005).
[11] E. T. Galloway and E. Herbst, Astron. Astrophys. **211**, 413 (1989).
[12] M. Shimizu, Astrophys. Space Sci. **36**, 353 (1975).
[13] J. M. Amero and G. J. Vázquez, Int. J. Quantum Chem. **99**, 353 (2004).
[14] K. Kawaguchi and T. Amano, J. Chem. Phys. **88**, 4584 (1988).
[15] R. Colin, J. Mol. Spectrosc. **136**, 387 (1989).
[16] U. Müller and G. Schulz, Chem. Phys. Lett. **170**, 401 (1990).
[17] A. Ehbrecht, A. Kowalski, and Ch. Ottinger, Int. J. Mass Spectrom. Ion Process. **173**, 127 (1998).
[18] J. M. Amero and G. J. Vázquez, Int. J. Quantum Chem. **101**, 396 (2005).
[19] I. Kusunoki, K. Yamashita, and K. Morokuma, Chem. Phys. Lett. **123**, 533 (1986).
[20] J. K. Park and H. Sun, Bull. Korean Chem. Soc. **11**, 34 (1990).
[21] J. K. Park and H. Sun, Chem. Phys. Lett. **211**, 618 (1993).
[22] J. Seong, J. K. Park, and H. Sung, Chem. Phys. Lett. **57**, 79 (1996).
[23] R. Tarroni, P. Palmieri, A. Mitrushenkov, P. Tosi, and D. Bassi, J. Chem. Phys. **106**, 10265 (1997).
[24] P. Q. Wang, A. M. Sayler, K. D. Carnes, J. F. Xia, M. A. Smith, B. D. Esry, and I. Ben-Itzhak, Phys. Rev. A **74**, 043411 (2006).
[25] P. Hansch and L. D. Van Woerkom, Opt. Lett. **21**, 1286 (1996).
[26] A. M. Sayler, P. Q. Wang, K. D. Carnes, and I. Ben-Itzhak, J. Phys. B **40**, 4367 (2007).
[27] A. M. Sayler, P. Q. Wang, K. D. Carnes, B. D. Esry, and I. Ben-Itzhak, Phys. Rev. A **75**, 063420 (2007).
[28] R. Marquardt, K. Sagui, W. Klopper, and M. Quack, J. Phys. Chem. B **109**, 8439 (2005).
[29] P. A. Orr, I. D. Williams, J. B. Greenwood, I. C. E. Turcu, W. A. Bryan, J. Pedregosa-Gutierrez, and C. W. Walter, Phys. Rev. Lett. **98**, 163001 (2007).
[30] A. Giusti-Suzor, F. H. Mies, L. F. DiMauro, E. Charron, and B. Yang, J. Phys. B **28**, 309 (1995).
[31] G. N. Gibson, L. Fang, and B. Moser, Phys. Rev. A **74**, 041401(R) (2006).
[32] A. Hishikawa, S. Liu, A. Iwasaki, and K. Yamanouchi, J. Chem. Phys. **114**, 9856 (2001).
[33] I. Ben-Itzhak, P. Q. Wang, J. F. Xia, A. M. Sayler, M. A. Smith, J. W. Maseberg, K. D. Carnes, and B. D. Esry, Nucl. Instrum. Methods Phys. Res. B **233**, 56 (2005).
[34] Estimating the maximum signal loss in channel $N^+ + D$, we extrapolate the exponential decay portion of Fig. 3(a) (i.e., KER > 0.1 eV) back to KER $= 0.0$ eV and integrate the relative yields of the extrapolated and observed data.
[35] M. V. Korolkov, H. G. Breunig, and K. M. Weitzel, Opt. Spectrosc. **103**, 325 (2007).